URSI GASS 2020, Rome, Italy, 29 August - 5 September 2020

Application of A GMMV-based Multi-frequency Inversion Method to 3-D Half-space Inverse Scattering Problems

Shilong Sun*(1), Dahai Dai(1), and Zhenhai Xu(1)
(1) College of Electronic Science, National University of Defense Technology, Changsha, 410073, China
Email: shilongsun@126.com

Abstract

As is well known, the inverse scattering theory is confronted with severe ill-posedness and huge computational burden when applied to 3-D half-space cases. In this paper, a GMMV-based multi-frequency inversion method is applied to solve 3-D half-space inverse scattering problems by exploiting the joint sparsity of the contrast sources with a multi-source multi-frequency measurement configuration. The computational complexity is acceptable, for the direct scattering problem is solved for just one time. Numerical simulation results demonstrate that this method is able to recover the location, shape and posture of 3-D targets with several frequency components, which is a promising attempt to extend the inversion theory to 3-D half-space inverse scattering problems.

1 Introduction

The inverse scattering theory is proposed primarily for tackling the scattering problems in the resonance region (the wavelengths and the dimension of the scatterers are comparable) [1, Chapter 1]. Differ from the imaging problems at high frequencies, inverse scattering problems in the resonance region show obvious nonlinearity and severe ill-posedness. The latter means minor perturbations of the scattered field pattern lead to large errors in the reconstruction of the scatterers. Moreover, for half-space inverse scattering problems, the scatterers can hardly be reconstructed due to the incomplete measurement of the field pattern, although regularization techniques are considered. Another obstacle is the huge computational complexity (especially for 3-D large-scale problems) for both global optimization techniques [2, 3, 4] and local optimization methods [5, 6]. Although doing inversion with neural networks is a promising idea that can greatly reduces the computational complexity, the generalization ability and stability of the current trained networks [7, 8] are still questionable. Actually the current end-to-end neural networks (a mapping from one image to the other) belong to a black box in which no physical regulation has been considered. In this paper, we introduce a multi-frequency inversion method based on the generalized multiple measurement vector (GMMV) model for solving the 3-D half-space inverse scattering problems. The joint sparsity of the contrast sources is exploited as a regularization constraint and the direct scattering problem is solved only once. Numerical simulation results demonstrate that this method is able to recover the location, shape and posture of 3-D targets with several frequencies, which is a promising attempt to extend the inversion theory to 3-D far field applications with a typical half-space configuration.

2 GMMV-based Multi-frequency Inversion

2.1 Formulation

The scattered field equation of 3-D inverse scattering problems is formulated as follows [9]

$$\nabla \times \mu_0^{-1} \nabla \times \boldsymbol{E}_{p,i}^{\mathrm{sct}} - \omega^2 \boldsymbol{\varepsilon}_{\mathrm{b}} \boldsymbol{E}_{p,i}^{\mathrm{sct}} = \omega_i^2 \boldsymbol{J}_{p,i}, \tag{1}$$

where, $p \in \{1,2,\cdots,P\}$ and $i \in \{1,2,\cdots,I\}$ are the indexes of the source positions and frequencies, respectively; $\boldsymbol{E}_p^{\mathrm{sct}}$ and $\boldsymbol{J}_p$ are the scattered electric field and the electric current source density, respectively; ω_i is the angular frequency; $\boldsymbol{\varepsilon}_b$ is the complex permittivity of the background medium. Note that the time factor used in this paper is $\exp(\mathrm{i}\omega_i t)$. All these quantities are functions of the position vector $\boldsymbol{x} = [x_1, x_2, x_3]$ and the angular frequency ω_i. Let us formulate the scattering operator with FDFD scheme and consider the measurements are spatial samples of the scattered field, the data equations is formulated as follows $\boldsymbol{f}_{p,i} = \boldsymbol{M}_p \boldsymbol{A}_i^{-1} \omega_i^2 \boldsymbol{j}_{p,i}$, where $\boldsymbol{M}_p$ is a spatial measurement matrix. Let us further reformulate the data equations as

$$\boldsymbol{Y} = \boldsymbol{\Phi} \cdot \boldsymbol{J} + \boldsymbol{U}, \tag{2}$$

where, $\boldsymbol{Y} = \begin{bmatrix} \boldsymbol{y}_{1,1} & \boldsymbol{y}_{2,1} & \cdots & \boldsymbol{y}_{P,1} & \boldsymbol{y}_{1,2} & \cdots & \boldsymbol{y}_{P,I} \end{bmatrix}$, $\boldsymbol{J} = \begin{bmatrix} \boldsymbol{j}_{1,1}^{\mathrm{ic}} & \boldsymbol{j}_{2,1}^{\mathrm{ic}} & \cdots & \boldsymbol{j}_{P,1}^{\mathrm{ic}} & \boldsymbol{j}_{1,2}^{\mathrm{ic}} & \cdots & \boldsymbol{j}_{P,I}^{\mathrm{ic}} \end{bmatrix}$, $\boldsymbol{j}_{p,i}^{\mathrm{ic}} = \omega_i \boldsymbol{j}_{p,i}$ is the normalized contrast source proportional to the induced current $\mathrm{i}\omega_i \mu_0 \boldsymbol{j}_{p,i}$; $\boldsymbol{\Phi} \cdot \boldsymbol{J}$ is defined by $\boldsymbol{\Phi} \cdot \boldsymbol{J} := \begin{bmatrix} \boldsymbol{\Phi}_{1,1} \boldsymbol{j}_{1,1}^{\mathrm{ic}} & \boldsymbol{\Phi}_{2,1} \boldsymbol{j}_{2,1}^{\mathrm{ic}} & \cdots & \boldsymbol{\Phi}_{P,I} \boldsymbol{j}_{P,I}^{\mathrm{ic}} \end{bmatrix}$, and correspondingly, $\boldsymbol{\Phi}^H \cdot \boldsymbol{Y}$ is defined as $\boldsymbol{\Phi}^H \cdot \boldsymbol{Y} := \begin{bmatrix} \boldsymbol{\Phi}_{1,1}^H \boldsymbol{y}_{1,1}^{\mathrm{ic}} & \boldsymbol{\Phi}_{2,1}^H \boldsymbol{y}_{2,1}^{\mathrm{ic}} & \cdots & \boldsymbol{\Phi}_{P,I}^H \boldsymbol{y}_{P,I}^{\mathrm{ic}} \end{bmatrix}$, where $\boldsymbol{\Phi}_{p,i} = \boldsymbol{M}_p \boldsymbol{A}_i^{-1} \omega_i$. Here, $\boldsymbol{Y} \in \mathbb{C}^{Q \times PI}$ is the data matrix, and the columns of $\boldsymbol{J} \in \mathbb{C}^{N \times PI}$ are the multiple vectors to be solved. $\boldsymbol{U} \in \mathbb{C}^{Q \times PI}$ represents the complex additive noises.

2.2 Solver framework

The GMMV model is solved by exploiting the joint sparsity of the normalized contrast sources [10]. Specifically, we solve a convex optimization problem (referred to as GMMV (BP_σ) problem) given by

$$\min_{\boldsymbol{J}} \quad \kappa(\boldsymbol{J}) \quad \text{s.t.} \quad \|\boldsymbol{\Phi}\cdot\boldsymbol{J}-\boldsymbol{Y}\|_F \le \sigma, \tag{3}$$

where, σ represents the noise level; $\kappa(\boldsymbol{J})$ is the mixed (α,β)-norm defined as

$$\|\boldsymbol{J}\|_{\alpha,\beta} := \left(\sum_{n=1}^{N} \|\boldsymbol{J}_{3n-2\rightarrow}\,\boldsymbol{J}_{3n-1\rightarrow}\,\boldsymbol{J}_{3n\rightarrow}\|_\beta^\alpha\right)^{1/\alpha}, \tag{4}$$

where, $\boldsymbol{J}_{n\rightarrow}$ denotes the n-th row vector of $\boldsymbol{J}$, and we select the mixed norm $\|\cdot\|_{1,2}$ as a regularized constraint. The solution to (3) can be found by solving several of the dual subproblem

$$\min_{\boldsymbol{J}} \quad \|\boldsymbol{\Phi}\cdot\boldsymbol{J}-\boldsymbol{Y}\|_F \quad \text{s.t.} \quad \kappa(\boldsymbol{J}) \le \tau, \tag{5}$$

and it is easy to have the derivation and proof of the spectral projected gradient (SPG) method by referring to [11, Section II.E]. With the estimation of $\boldsymbol{J}$, and hence $\hat{\boldsymbol{e}}^{\mathrm{tot}}_{p,i}$, the contrast $\boldsymbol{\chi}=\boldsymbol{\chi}_1$ is obtained by minimizing the cost function

$$C = \sum_{i=1}^{N_f}\eta_{1,i}\sum_{p=1}^{P}\left\|\boldsymbol{y}_{p,i}-\boldsymbol{\Phi}_{p,i}\hat{\boldsymbol{e}}^{\mathrm{tot}}_{p,i}\left(\Re\{\boldsymbol{\chi}\}+\frac{\omega_1}{\omega_i}\Im\{\boldsymbol{\chi}\}\right)\right\|_2^2 + \sum_{i=1}^{N_f}\eta_{2,i}\sum_{p=1}^{P}\left\|\hat{\boldsymbol{e}}^{\mathrm{tot}}_{p,i}\left(\Re\{\boldsymbol{\chi}\}+\frac{\omega_1}{\omega_i}\Im\{\boldsymbol{\chi}\}\right)-\hat{\boldsymbol{j}}^{\mathrm{ic}}_{p,i}\right\|_2^2, \tag{6}$$

where,

$$\eta_{1,i}=1\Big/\sum_{p=1}^{P}\|\boldsymbol{y}_{p,i}\|_2^2\,,\ \eta_{2,i}=1\Big/\sum_{p=1}^{P}\|\boldsymbol{e}^{\mathrm{inc}}_{p,i}\boldsymbol{\chi}_i\|_2^2\,. \tag{7}$$

3 Simulation Results

In this section, a 3-D half-space inverse scattering simulation is given to demonstrate the validity of the proposed method. Figure 1 gives the geometry of this numerical experiment. The planar antenna array consists of 4×4 ideal electric dipole transmitting antennas and 10×10 receiving antennas. The source consists of an x-polarized electric dipole and a y-polarized one. A circular polarized wave is generated by introducing a $\pi/2$ phase shift between the two dipoles. The x- and y-components of the electric fields are measured simultaneously. Namely, we have a data matrix $\boldsymbol{Y}_i\in\mathbb{C}^{200\times16}$ at one frequency. The targets includes one metallic circular cylinder and a triangular cylinder ($\varepsilon_\mathrm{r}=4$, $\sigma=0.05$ S/m). Due to the huge computational resource requirement, we considered a limited 3-D domain in which the numerical experiment is a near field inverse scattering problem when metre-wave is considered. However, the distances between the antennas and the targets can be extended to several or even hundreds of kilometers, which is a typical far field inverse scattering problem, while the proposed method is still applicable.

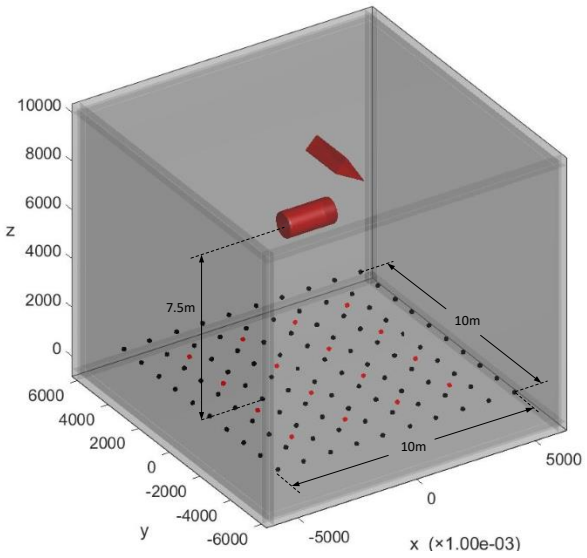

Figure 1. Targets include a metallic circular cylinder and a lossy triangular cylinder ($\varepsilon_\mathrm{r}=4$, $\sigma=0.05$ S/m). Red/black points represent the transmitting/receiving antennas, respectively.

The direct 3-D scattering problem is solved by a MATLAB-based 3-D FDFD package 'MaxwellFDFD' and its companion C program "FD3D"[12]. The inversion domain is restricted to the region $[-4,4]\times[-4,4]\times[6,10]$ m^3 and is uniformly discretized by $131\times131\times70$ grids. We processed five frequencies at 100 MHz, 150 MHz, 200 MHz, 250 MHz and 300 MHz, simultaneously. Figure 2 (a) and (b) respectively show the geometry of the real objects and the reconstructed contrast when signal to noise ratio (SNR) is 25 dB. Slices of the reconstructed permittivity and conductivity are given by Figure 3. On one hand, the result has demonstrated that this method is able to recover the location, shape and posture of 3-D targets with several frequency components. On the other hand, the estimated values of the dielectric parameters are far from the real ones, because 1) only a small fraction of the field pattern is available for the half-space configuration; 2) the formulation of the problem has been simplified to reduce the computational complexity. We have also tested the method when SNR is reduced to 0 dB and the result is given by Figure 2(c), from which we see the inversion result is still acceptable when SNR is poor, although false targets have been reconstructed beneath and above the real position of the targets. It is worth noting that a cross-validation technique is used, such that the noise level σ in (3) can be adaptively adjusted. We run the code on a workstation with 32 CPU cores, and the total running time is less than 1 hour with the parallel computing technique.

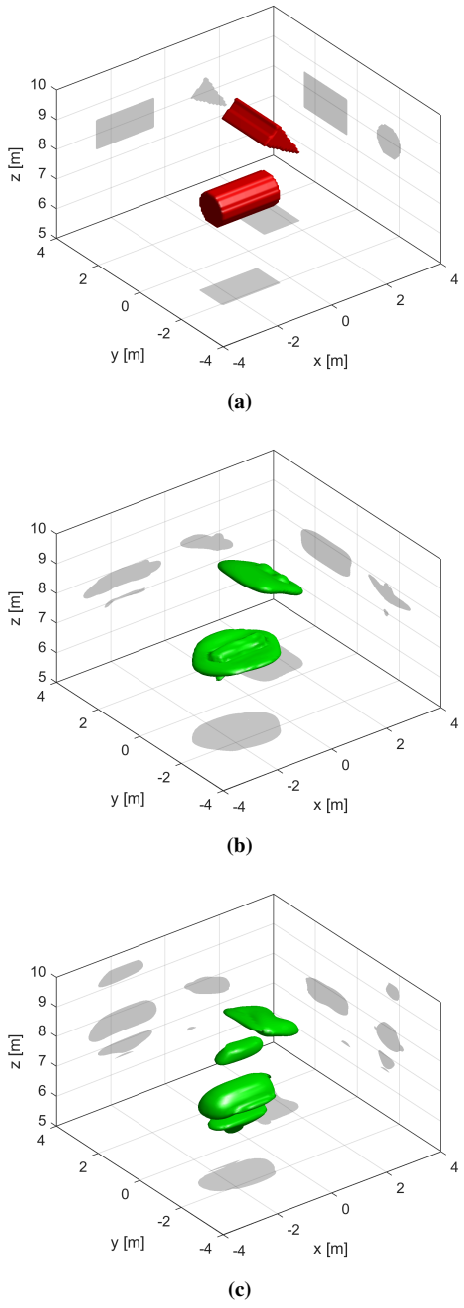

Figure 2. Geometry of the real objects (a) and the reconstructed contrast when SNR is 25 dB (b) and 0 dB (c) with five frequencies — 100 MHz, 150 MHz, 200 MHz, 250 MHz and 300 MHz.

4 Conclusion

In this paper, we studied the application of a GMMV-based multi-frequency inversion method to 3-D half-space inverse scattering problems. Numerical results demonstrate that the location, shape and posture of 3-D targets can be recovered with several frequency components. We also need to remark that more work is required to further improve the estimation accuracy of the dielectric parameter, which is of great importance for target recognition.

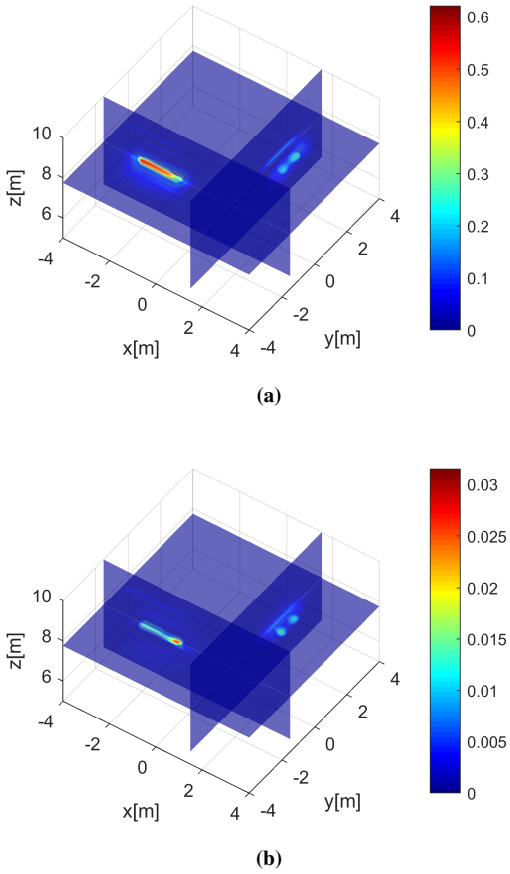

Figure 3. Slices of the reconstructed permittivity (a) and conductivity (b) with five frequencies — 100 MHz, 150 MHz, 200 MHz, 250 MHz and 300 MHz. SNR is 25 dB.

References

[1] D. Colton and R. Kress, *Inverse acoustic and electromagnetic scattering theory*, vol. 93. Springer Science & Business Media, 2012.

[2] S. Caorsi, A. Massa, and M. Pastorino, "A crack identification microwave procedure based on a genetic algorithm for nondestructive testing," *IEEE Transactions on Antennas and Propagation*, vol. 49, no. 12, pp. 1812–1820, 2001.

[3] P. Rocca, M. Benedetti, M. Donelli, D. Franceschini, and A. Massa, "Evolutionary optimization as applied to inverse scattering problems," *Inverse Problems*, vol. 25, no. 12, p. 123003 (41pp), 2009.

[4] M. Salucci, L. Poli, N. Anselmi, and A. Massa, "Multifrequency particle swarm optimization for enhanced multiresolution GPR microwave imaging," *IEEE Transactions on Geoscience and Remote Sensing*, vol. 55, no. 3, pp. 1305–1317, 2017.

[5] P. M. Van Den Berg and R. E. Kleinman, "A contrast source inversion method," *Inverse problems*, vol. 13, no. 6, p. 1607, 1997.

[6] S. Sun, B. J. Kooij, T. Jin, and A. G. Yarovoy, "Cross-correlated contrast source inversion," *IEEE Transactions on Antennas and Propagation*, vol. 65, no. 5, pp. 2592–2603, 2017.

[7] L. Li, L. G. Wang, F. L. Teixeira, C. Liu, A. Nehorai, and T. J. Cui, "DeepNIS: Deep neural network for nonlinear electromagnetic inverse scattering," *IEEE Transactions on Antennas and Propagation*, 2018.

[8] Z. Wei and X. Chen, "Deep-learning schemes for full-wave nonlinear inverse scattering problems," *IEEE Transactions on Geoscience and Remote Sensing*, vol. 57, no. 4, pp. 1849–1860, 2018.

[9] S. Sun, B. J. Kooij, and A. G. Yarovoy, "Linearized three-dimensional electromagnetic contrast source inversion and its applications to half-space configurations," *IEEE Transactions on Geoscience and Remote Sensing*, vol. 55, no. 6, pp. 3475–3487, 2017.

[10] E. van den Berg and M. P. Friedlander, "Probing the pareto frontier for basis pursuit solutions," *SIAM Journal on Scientific Computing*, vol. 31, no. 2, pp. 890–912, 2008.

[11] S. Sun, B. J. Kooij, and A. G. Yarovoy, "A linear model for microwave imaging of highly conductive scatterers," *IEEE Transactions on Mcrowave Theorey and Techniques*, vol. PP, no. 99, pp. 1–16, 2017.

[12] W. Shin, "MaxwellFDFD Webpage," 2015. https://github.com/wsshin/maxwellfdfd.